S. Ishiwata and Y. Matsunaga, Editors
Physics of Self-Organization Systems
(World Scientific, New Jersey, 2008) pp. 67-87

THERMODYNAMIC TIME ASYMMETRY AND NONEQUILIBRIUM STATISTICAL MECHANICS

Pierre GASPARD

Center for Nonlinear Phenomena and Complex Systems,
Université Libre de Bruxelles, Code Postal 231, Campus Plaine, B-1050 Brussels,
Belgium

A review of recent advances in nonequilibrium statistical mechanics is presented. These new results explain how the time reversal symmetry is broken in the statistical description of nonequilibrium processes and the thermodynamic entropy production finds its origin in the time asymmetry of nonequilibrium fluctuations. These advances are based on new relationships expressing the time asymmetry in terms of the temporal disorder and the probability distributions of nonequilibrium fluctuations. These relationships apply to driven Brownian motion and molecular motors.

Keywords: microreversibility, entropy production, relaxation, diffusion, out-of-equilibrium nanosystems.

1. Introduction

Nonequilibrium statistical mechanics is undergoing tremendous advances with the discovery of universal relationships ruling molecular fluctuations near and far from equilibrium. These new relationships have been discovered thanks to dynamical systems theory where new concepts have been introduced to understand chaotic behavior. In this context, the issue of the initial conditions of a dynamical system has been discussed about the phenomenon of sensitivity to initial conditions. The focus on this issue have disclosed striking features on the role of initial conditions in the time asymmetry of nonequilibrium processes.

It is our purpose to give an overview of these recent results and their applications to out-of-equilibrium nanosystems. Indeed, at the nanoscale, the fluctuations can no longer be neglected as it is the case at the macroscale. Accordingly, the processes taking place in nanosystems should be described in terms of the probability distributions of molecular fluctuations. The fact

is that many nanosystems find their relevance because they function under nonequilibrium conditions, as for molecular motors or electronic conducting nanodevices. The new advances in nonequilibrium statistical mechanics thus establish the bases for a statistical thermodynamics of out-of-equilibrium nanosystems. Remarkably, these recent developments provide an unprecedented insight into our understanding of biological phenomena from the viewpoint of statistical thermodynamics. This insight extends much beyond the already important results obtained with the macroscopic thermodynamics of irreversible processes [1], which did not deal with the fluctuations and their temporal properties. By carrying out the connection between the macroscale and the molecular aspects at the nanoscale, nonequilibrium statistical mechanics is nowadays able to bridge the gaps between molecular biology, bioenergetics, and the thermodynamic laws thanks to the advent of the new results about nonequilibrium fluctuations.

The review is organized as follows. The breaking of time reversal symmetry in nonequilibrium statistical mechanics is discussed in Sec. 2 and illustrated in Sec. 3 with the relaxation modes of diffusion. We explain in Sec. 4 how the thermodynamic arrow of time finds its origin in the time asymmetry of temporal disorder in nonequilibrium fluctuations. In Sec. 5, we give an overview of the so-called fluctuation theorems. The case of molecular motors is presented in Sec. 6. Conclusions and perspectives are given in Sec. 7.

2. The breaking of time reversal symmetry in nonequilibrium statistical mechanics

The second law of thermodynamics is expressed in terms of the concept of entropy. This quantity was interpreted by Boltzmann as a characterization of the disorder in the probability distribution of the positions and velocities of the particles composing the system. Later, Gibbs pointed out that the microscopic definition of entropy requires coarse graining in one way or another. There exist different versions of coarse graining. The first was introduced by Boltzmann who obtained his famous H-theorem by describing dilute gases in terms of one-particle distributions. In this way, he neglected the statistical correlations between several particles, which may be justified for dilute gases but allows the corresponding entropy to vary in time. Another version consists in tracing out the degrees of freedom of the environment of a subsystem, as done for a Brownian particle. *In fine*, the phase space can be partitioned into grains or cells to get the occupation probabilities of these cells, as suggested by Gibbs in 1902. Since the work

of Sadi Carnot, coarse graining is inherently associated with the idea of entropy because the efficiency of steam engines is a property of the steam microscopic degrees of freedom manipulated by some macroscopic piston on a very coarse-grained level. Only the coarse-grained entropy may evolve in time as the consequence of the dynamical property of mixing, also introduced by Gibbs. Indeed, the fine-grained entropy remains constant in time.

However, the breaking of the time reversal symmetry can be formulated in nonequilibrium statistical mechanics at a more fundamental level without referring from the start to the thermodynamic entropy, but instead discussing the symmetry of the probability distribution of the positions $\mathbf{r}$ and velocities $\mathbf{v}$ of the particles in classical mechanics:

$$p(\mathbf{\Gamma}; t) = p(\mathbf{r}, \mathbf{v}; t) \tag{1}$$

or the matrix density in quantum mechanics. These quantities obey time evolution equations that is the Liouville equation for classical systems:

$$\partial_t \, p = \{H, p\}_{\text{Poisson}} \equiv \hat{L} \, p \tag{2}$$

where $\{H, \cdot\}_{\text{Poisson}}$ denotes the Poisson bracket with the Hamiltonian function H, or the Landau-von Neumann equation for quantum systems. Actually, the time evolution of the probability distribution is induced by the deterministic equations of motion which are Newton's or Hamilton's equations of classical mechanics and Schrödinger's equation of quantum mechanics. These equations are deterministic in the sense that their solutions are uniquely given in terms of their initial conditions according to Cauchy's theorem. In classical systems, the initial condition is a point $\mathbf{\Gamma} = (\mathbf{r}, \mathbf{v})$ taken in the phase space of the positions and velocities of the particles while the initial condition is a wavefunction taken in the Hilbert space of a quantum system.

Probability distributions are introduced because the initial state can never be prepared with an infinite precision on uncountable continua such as phase spaces or Hilbert spaces. On such continua, there is always a dichotomy between the existence of a point-like initial condition and the necessarily unprecise knowledge of this latter. As a result, the predictability of the trajectory becomes a concern in systems with sensitivity to initial conditions – the so-called chaotic systems. Dynamical chaos guarantees Gibbs' mixing property, which allows us to understand relaxation processes in many systems. It is also important to justify the use of a statistical description in terms of probability distributions beyond the Lyapunov time characteristic of the sensitivity to initial conditions [2].

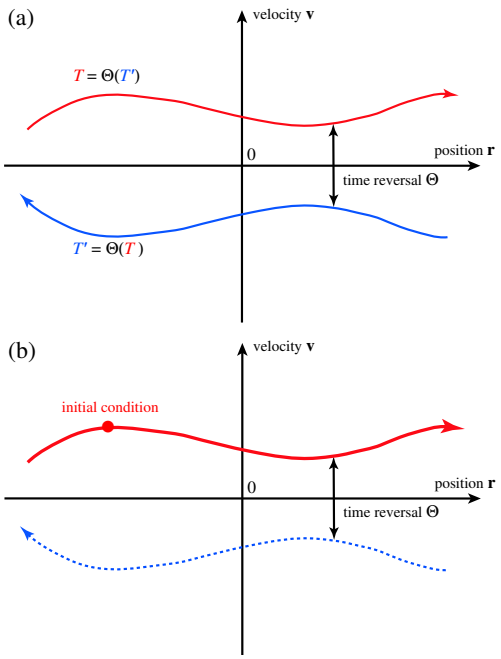

Fig. 1. (a) If Newton's equation is time reversal symmetric, the time reversal $\Theta(T)$ of every solution T is also a solution, as here shown in the phase space of the positions and velocities of the system. (b) If the time reversal $\Theta(T)$ is physically distinct from the trajectory T, the selection of the trajectory T by the initial condition gives a unit probability to T and zero to all the other solutions including the time reversal image $\Theta(T)$, therefore breaking the time reversal symmetry.

It turns out that the breaking of time reversal symmetry is another issue concerning the initial conditions in chaotic as well as non-chaotic systems, as shown by the following discussion carried out in the framework of classical mechanics. It is well known that Newton's equation is symmetric under time reversal:

$$\Theta(\mathbf{r}, \mathbf{v}) = (\mathbf{r}, -\mathbf{v}) \tag{3}$$

which leaves the positions $\mathbf{r}$ unchanged and reverses the velocities $\mathbf{v} = d\mathbf{r}/dt$, if the Hamiltonian is an even function of the velocities. The symmetry – called microreversibility – means that the time reversal of a solution of Newton's equation is also a solution of this equation (see Fig. 1a). Each initial condition selects a precise solution of Newton's equations, which depicts a trajectory $T = \{\mathbf{\Gamma}(t) | t \in \mathbb{R}\}$ in the phase space $\mathbf{\Gamma} = (\mathbf{r}, \mathbf{v})$. We may say that a trajectory T is *physically distinct* from another trajectory

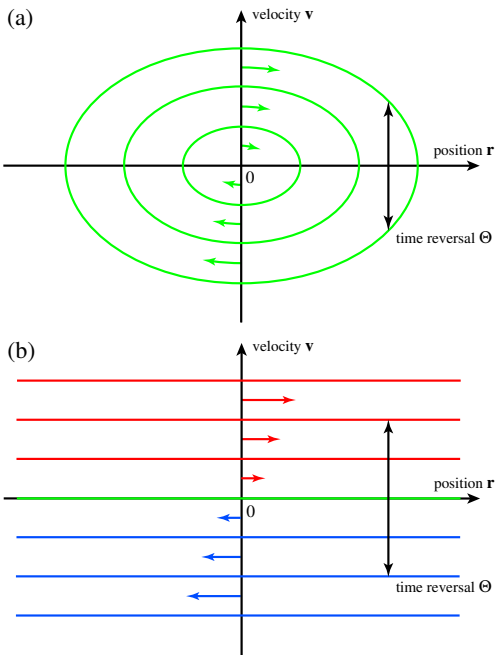

Fig. 2. (a) Phase portrait of the harmonic oscillator (4). All its trajectories are ellipses which are self-reversed. Consequently, the selection of an initial condition does not break the time reversal symmetry in this system. (b) Phase portrait of the free particle (5). Here, the trajectories are physically distinct from their image under time reversal, except if the velocity vanishes. Consequently, the selection of an initial condition (with a non-vanishing velocity) breaks the time reversal symmetry in this system.

if they do not coincide in the phase space of the system.

If the trajectory T followed by the system during its time evolution is physically distinct from its time reversal, $\Theta(T) \neq T$, it turns out that the time reversal symmetry is broken in the system. This is the same as for other symmetry breaking phenomena in condensed matter physics. For instance, the double-well potential $V(x) = (x^2/2) - (x^4/4)$ is symmetric under parity $x \to -x$. This symmetry is broken if the system is found in one of the wells, either $x = +1$ or $x = -1$. This illustrates the general result that the solution of an equation may have a lower symmetry than the equation itself. This phenomenon of symmetry breaking applies to time reversal as well. Although Newton's equation is time reversal symmetric, its solutions do not necessarily have the symmetry. Therefore, the selection of a trajectory by the initial condition can break the time reversal symmetry.

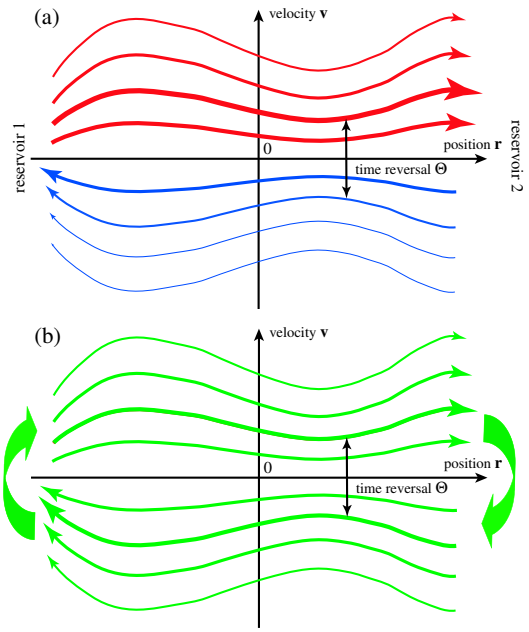

Fig. 3. (a) Phase portrait of a nonequilibrium system with particles diffusing between the high concentration reservoir 1 and the low concentration reservoir 2. The trajectories from 1 to 2 typically have a higher probability weight than the trajectories from 2 to 1 in order that the mean current flows from 1 to 2. The probability weight is indicated by the thickness of the trajectories, showing the time asymmetry of the probability distribution. (b) Phase portrait at equilibrium if the contacts with the reservoirs are closed, in which case detailed balance is satisfied and the probability distribution is time reversal symmetric.

This happens if the trajectory selected by the initial condition is physically distinct from its time reversal (see Fig. 1b).

This time reversal symmetry breaking does not manifest itself in every system. In particular, all the trajectories of Newton's equation:

$$m\frac{d^2r}{dt^2} = -kr \tag{4}$$

of the harmonic oscillator are the ellipses $E = (mv^2 + kr^2)/2$ in the phase space (r, v). Each ellipsis is mapped onto itself by time reversal $\Theta(r, v) = (r, -v)$. All the trajectories are thus self-reversed in the harmonic oscillator (see Fig. 2a). In contrast, almost all the trajectories are distinct from their time reversal in the case of the free particle of Newton's equation:

$$m\frac{d^2r}{dt^2} = 0 \tag{5}$$

Indeed, the trajectories are the straight lines $r(t) = r(0)+v(0)t$, $v(t) = v(0)$, which are distinct from their reversal if the velocity is non vanishing, $v(0) \neq 0$ (see Fig. 2b). Therefore, the selection of an initial condition may already break the time reversal symmetry in this simple system. *A fortiori*, this breaking can also happen in a chaotic system with a spectrum of positive Lyapunov exponents indicating many stable and unstable directions in phase space. These directions are mapped onto each other but physically distinct so that the time reversal symmetry will be broken if one specific direction is selected by the initial condition [3,4].

In statistical mechanics, each initial condition – and thus each phase-space trajectory – is weighted with a probability giving its statistical frequency of occurrence in a sequence of repeated experiments. This is in particular the case for a nonequilibrium system with particles diffusing between two reservoirs at different concentrations. After some transients, the system reaches a nonequilibrium steady state which can be described by an invariant probability distribution. Averaging over this distribution gives a mean current of diffusing particles from high to low concentrations. In this case, the phase-space trajectories issued from the high concentration reservoir typically have a higher probability weight than the trajectories from the low concentration reservoir (see Fig. 3a). Since the set of these latter trajectories contain the time reversal of the former ones, we conclude that the time reversal symmetry is broken by the nonequilibrium invariant probability distribution:

$$p_{\rm neq}(\Theta\mathbf{\Gamma}) \neq p_{\rm neq}(\mathbf{\Gamma}) \tag{6}$$

Of course, if the contacts with the reservoirs are closed, the invariant probability becomes the equilibrium one after relaxation, in which case detailed balance is satisfied and the time reversal symmetry is restored:

$$p_{\rm eq}(\Theta\mathbf{\Gamma}) = p_{\rm eq}(\mathbf{\Gamma}) \tag{7}$$

(see Fig. 3b). Since the nonequilibrium invariant probability distributions are stationary solutions of Liouville's equation (2), we here have a similar symmetry breaking phenomenon as for Newton's equation. The nonequilibrium stationary density (6) is a solution of Liouville's equation with a lower symmetry than the equation itself. In this way, irreversible behavior can be described by weighting differently the trajectories T and their time reversal images $\Theta(T)$ with a probability measure.

3. The relaxation modes of diffusion

In this section, we show in specific systems that the breaking of time reversal symmetry is indeed the fact of systems in nonequilibrium states. We consider Hamiltonian systems with chaotic diffusion such as the multibaker map [5–7], the hard-disk Lorentz gas, and the Yukawa-potential Lorentz gas [8]. The Newtonian dynamics of these systems is Hamiltonian and time reversal symmetric. These systems sustain the transport property of diffusion because of their spatial extension. Moreover, the dynamics is periodic in space as for the motion of electrons or impurities in a crystal.

If the initial conditions are taken out of equilibrium, the probability distribution undergoes a transient relaxation toward a uniform state corresponding to the thermodynamic equilibrium. This relaxation can be decomposed into modes which are special solutions of Liouville's equation (2):

$$p(\mathbf{r}, \mathbf{v}; t) = C \exp(s_{\mathbf{k}} t)\, \Psi_{\mathbf{k}}(\mathbf{r}, \mathbf{v}) \tag{8}$$

These solutions are spatially periodic $\Psi_{\mathbf{k}}(\mathbf{r}, \mathbf{v}) \sim \exp(i\mathbf{k} \cdot \mathbf{r})$ with a wavelength $\lambda = 2\pi/k$ typically much longer than the periodicity of the crystal. The solutions (8) are exponentially damped in time at the rate

$$-s_{\mathbf{k}} = \mathcal{D}\mathbf{k}^2 + O(\mathbf{k}^4) \tag{9}$$

vanishing quadratically with the wavenumber $\mathbf{k}$, which defines the diffusion coefficient given by the Green-Kubo formula:

$$\mathcal{D} = \int_0^\infty \langle v_x(0) v_x(t) \rangle_{\mathrm{eq}}\, dt \tag{10}$$

It turns out that the relaxation modes (8) can be constructed in phase space as generalized eigenstates of the Liouvillian operator of Eq. (2):

$$\hat{L}\, \Psi_{\mathbf{k}} = s_{\mathbf{k}} \Psi_{\mathbf{k}} \tag{11}$$

with the associated eigenvalue $s_{\mathbf{k}}$ given by a so-called Pollicott-Ruelle resonance [2]. The generalized eigenstates $\Psi_{\mathbf{k}}$ do not exist as functions but as distributions of Schwartz type, which are defined on some functional space of test functions. The remarkable feature of the construction is that it can be carried out without a specific coarse graining since the distribution $\Psi_{\mathbf{k}}$ is defined on a whole functional space of possible test functions. The use of such test functions may be considered as coarse graining but the generalized eigenstate does not depend on the choice of a specific test function taken in the functional space.

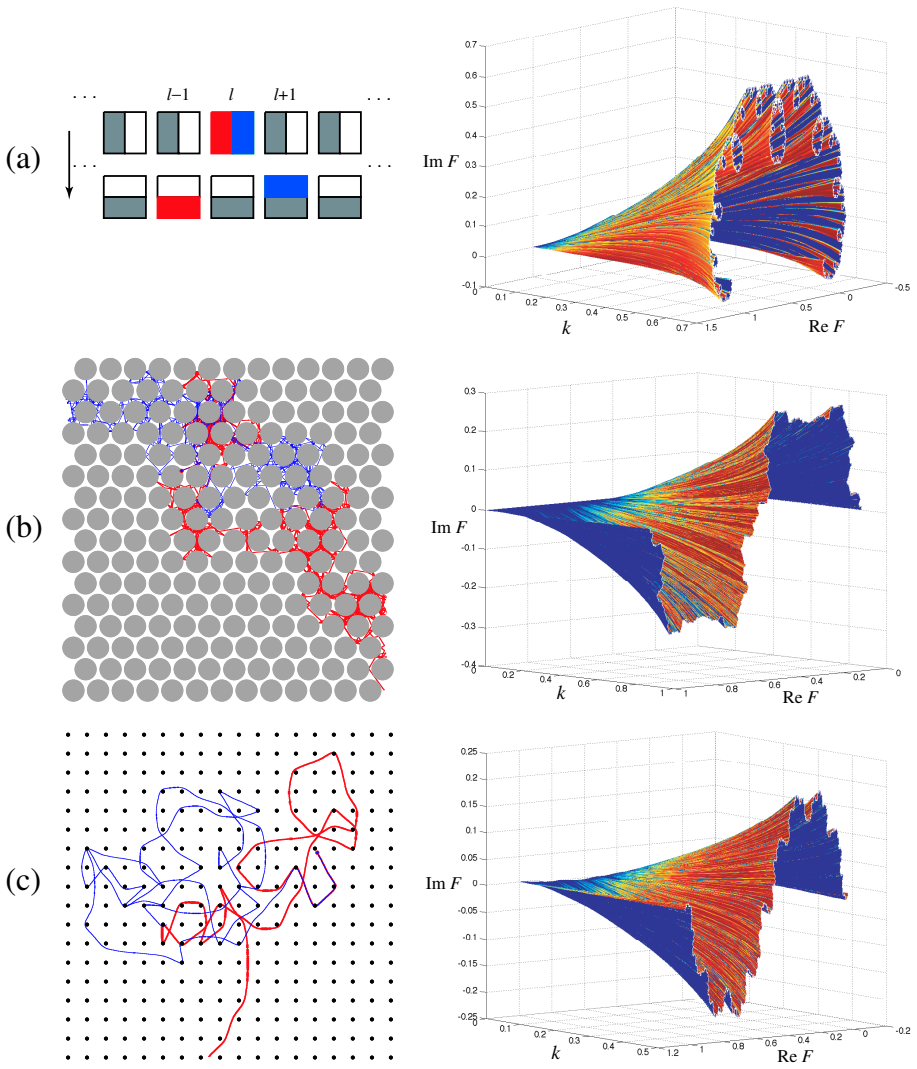

Fig. 4. The relaxation modes of diffusion in (a) the multibaker map [5–7], (b) the hard-disk Lorentz gas, and (c) the Yukawa-potential Lorentz gas [8]. The left-hand column shows the mechanism of diffusion of particles in these systems. In the right-hand column, the cumulative function (12) is depicted in the complex plane $(\mathrm{Re}\, F, \mathrm{Im}\, F)$ versus the wavenumber k, for each system. If the wavenumber vanishes $k = 0$, the cumulative function reduces to the straight line $\mathrm{Im}\, F = 0$ between the points $\mathrm{Re}\, F = 0$ and $\mathrm{Re}\, F = 1$, which represents the microcanonical equilibrium state.

The densities $\Psi_{\mathbf{k}}(\mathbf{r},\mathbf{v})$ are singular along the stable manifolds $W_{\rm s}$ of phase space, but nevertheless smooth along the unstable manifolds $W_{\rm u}$. Since the stable and unstable manifolds are mapped onto each other by time reversal $W_{\rm u}=\Theta(W_{\rm s})$, but are physically distinct $W_{\rm u}\neq W_{\rm s}$, the densities $\Psi_{\mathbf{k}}(\mathbf{r},\mathbf{v})$ are solutions of Liouville's equation which break the time reversal symmetry, as expected for solutions corresponding to unidirectional exponential decay. The time asymmetry of the relaxation modes can be displayed by explicitly constructing the eigenstates thanks to their cumulative function

$$F_{\mathbf{k}}(\theta)=\int_0^\theta \Psi_{\mathbf{k}}(\mathbf{r}_{\theta'},\mathbf{v}_{\theta'})\,d\theta'=\lim_{t\to\infty}\frac{\int_0^\theta \exp\left[i\mathbf{k}\cdot(\mathbf{r}_t-\mathbf{r}_0)_{\theta'}\right]\,d\theta'}{\int_0^{2\pi}\exp\left[i\mathbf{k}\cdot(\mathbf{r}_t-\mathbf{r}_0)_{\theta'}\right]\,d\theta'} \tag{12}$$

obtained by integrating their density $\Psi_{\mathbf{k}}(\mathbf{r},\mathbf{v})$ over some line $(\mathbf{r}_\theta,\mathbf{v}_\theta)$ in phase space [8]. Because of the singular character of the density in the stable directions, these cumulative functions depict fractal curves in the complex plane $(\mathrm{Re}\,F_{\mathbf{k}},\mathrm{Im}\,F_{\mathbf{k}})$. These fractal curves are depicted in Fig. 4 for the multibaker map [5–7] and the aforementioned Lorentz gases [8].

The fractal dimension $D_{\rm H}$ of these curves is given by the root of the equation [8]:

$$\mathcal{D}\mathbf{k}^2\simeq-\mathrm{Re}\,s_{\mathbf{k}}=\lambda(D_{\rm H})-\frac{h(D_{\rm H})}{D_{\rm H}} \tag{13}$$

where $\mathcal{D}$ is the diffusion coefficient while λ and h are the positive Lyapunov exponent and the Kolmogorov-Sinai entropy per unit time defined at the value $D_{\rm H}$ of the fractal dimension. Given that the Kolmogorov-Sinai entropy tends to the Lyapunov exponent as the fractal dimension approaches unity, this latter becomes

$$D_{\rm H}=1+\frac{\mathcal{D}}{\lambda}\,\mathbf{k}^2+O(\mathbf{k}^4) \tag{14}$$

for small values of the wavenumber [8]. Since the relaxation modes are singular in the stable directions but smooth in the unstable ones, the fractal character of their cumulative function is the direct manifestation of the breaking of the time reserval symmetry by these modes.

We notice that Eq. (13) is an extension of the escape-rate formulae giving each transport coefficient in terms of the Lyapunov exponents and the Kolmogorov-Sinai entropy per unit time on a fractal repeller [9,10]. Already in this framework, the escape rate is associated with nonequilibrium decaying states which break the time reversal symmetry.

The density of the nonequilibrium steady state of gradient $\mathbf{g}$ can be obtained from the densities (8) of the relaxation modes according to

$$\Psi_{\mathbf{g}}(\mathbf{\Gamma}) = -i\mathbf{g}\cdot\frac{\partial}{\partial\mathbf{k}}\Psi_{\mathbf{k}}(\mathbf{\Gamma})\Big|_{\mathbf{k}=0} = \mathbf{g}\cdot\left[\mathbf{r}(\mathbf{\Gamma}) + \int_0^{-\infty}\mathbf{v}(\mathbf{\Phi}^t\mathbf{\Gamma})\,dt\right] \qquad (15)$$

where $\mathbf{\Phi}^t$ denotes the Hamiltonian flow [6]. Because of Eq. (15), the nonequilibrium steady states have similar singularities as the relaxation modes. Their distribution is smooth along the unstable manifolds but singular in the stable directions. Their cumulative function is the nondifferentiable Takagi function in the multibaker map and its generalizations in the Lorentz gases [6]. This singular character is thus the manifestation of the breaking of the time reversal symmetry by the invariant probability distribution of nonequilibrium steady states.

4. Experimental evidence of the time asymmetry of nonequilibrium fluctuations

The breaking of the time reversal symmetry by the invariant probability distribution describing the nonequilibrium steady states has direct experimental consequences, which have been evidenced in recent experiments in the group of Professor Sergio Ciliberto at the ENS of Lyon (France) on the driven Brownian motion of a micrometric particle trapped by an optical tweezer in a moving fluid and the Nyquist thermal noise of a RC electric circuit driven out of equilibrium by a current [11,12].

In driven Brownian motion, the position of the particle can be monitored with nanometric resolution thanks to an interferometer. Long time series of the position of the Brownian particle have been recorded in the frame of the optical trap for a driving by the surrounding fluid with the speeds u and $-u$. Examples of such paths are depicted in Fig. 5a. Figure 5b gives the corresponding stationary probability distributions of the position z, showing the effect of the drag due to the moving fluid. The observations are well described by an overdamped Langevin equation including the force exerted by the potential of the laser trap, the drag force of the moving fluid, the viscous firction force, and the Langevin force of the thermal fluctuations [11,12]. The long time series allow us to measure the probabilities of paths $\boldsymbol{\omega} = \omega_0\omega_1\omega_2\ldots\omega_{n-1}$ of varying resolution ε on the position and sampled every time interval τ. We can compare the probability of a path in the process of speed u with the probability of the time-reversed path $\boldsymbol{\omega}^{\rm R} = \omega_{n-1}\ldots\omega_2\omega_1\omega_0$ in the process of opposite speed $-u$. As for the trajectories, a time-reversed path is typically distinct from the corresponding path, $\boldsymbol{\omega}^{\rm R} \neq$

$\boldsymbol{\omega}$. The coincidence only happens for the rare self-reversed paths. According to detailed balance, we expect that the probabilities of the paths and their time reversal are equal if $u = 0$:

$$\text{equilibrium:} \qquad P_0(\omega_0\omega_1 \dots \omega_{n-1}) = P_0(\omega_{n-1} \dots \omega_1\omega_0) \tag{16}$$

However, this equality is not expected if $u \neq 0$:

$$\text{out of equilibrium:} \qquad P_u(\omega_0\omega_1 \dots \omega_{n-1}) \neq P_{-u}(\omega_{n-1} \dots \omega_1\omega_0) \tag{17}$$

This difference also affects the decay of these path probabilities. Their mean decay rates characterize the temporal disorder or dynamical randomness and are called the (ε, τ)-entropy per unit time [13]:

$$h = \lim_{n\to\infty} -\frac{1}{n\tau} \sum_{\omega_0\omega_1\dots\omega_{n-1}} P_u(\omega_0\omega_1 \dots \omega_{n-1}) \ln P_u(\omega_0\omega_1 \dots \omega_{n-1}) \tag{18}$$

and time-reversed (ε, τ)-entropy per unit time [14]:

$$h^{\mathrm{R}} = \lim_{n\to\infty} -\frac{1}{n\tau} \sum_{\omega_0\omega_1\dots\omega_{n-1}} P_u(\omega_0\omega_1 \dots \omega_{n-1}) \ln P_{-u}(\omega_{n-1} \dots \omega_1\omega_0) \tag{19}$$

The supremum of the dynamical entropy (18) over all the possible coarse grainings defines the famous Kolmogorov-Sinai entropy per unit time, which equals the sum of positive Lyapunov exponents in closed dynamical systems according to Pesin's theorem [2]. Instead, the time-reversed entropy per unit time (19) has been recently introduced motivated by the difference (17) expected in nonequilibrium processes [14]. Contrary to the thermodynamic entropy which measures the disorder of the probability distribution in the phase space at a given time, the entropies per unit time characterize the disorder displayed by the process along the time axis, as in the successive pictures of a movie. We thus speak of temporal disorder or dynamical randomness for the property characterized by the quantities (18) and (19). To avoid a possible confusion with the standard thermodynamic entropy, we shall respectively call them the forward and reversed randomnesses in the following.

The most remarkable result is that the difference between these randomnesses gives the thermodynamic entropy production according to

$$\frac{1}{k_{\mathrm{B}}} \frac{d_{\mathrm{i}}S}{dt} = \lim_{\varepsilon,\tau\to 0} \left[h^{\mathrm{R}}(\varepsilon, \tau) - h(\varepsilon, \tau)\right] \geq 0 \tag{20}$$

where k_{B} is Boltzmann's constant [14]. This difference is the Kullback-Leibler distance between the path probabilities $P_u(\boldsymbol{\omega})$ and $P_{-u}(\boldsymbol{\omega}^{\mathrm{R}})$, also

known under the name of relative entropy, and is therefore always nonnegative in agreement with the second law of thermodynamics. The formula (20) is remarkable because it connects the arrow of time of macroscopic thermodynamics to another arrow of time observed at the mesoscopic scales in the temporal disorder of the nonequilibrium fluctuations. The time asymmetry of this temporal disorder manifests itself in the difference $h^{\mathrm{R}} - h$. The formula (20) thus shows that the thermodynamic arrow of time finds its origin in the time asymmetry of temporal disorder in the nonequilibrium fluctuations.

The formula (20) is also remarkable because it provides a rational foundation to the intuitive idea that dynamical order arises in a system driven out of equilibrium, as expressed by the

Theorem of nonequilibrium temporal ordering [15]: *In nonequilibrium steady states, the typical paths are more ordered in time than their corresponding time reversals in the sense that their temporal disorder characterized by h is smaller than the temporal disorder of the corresponding time-reversed paths characterized by h^{R}.*

This theorem expresses the fact that the molecular motions are completely erratic at equilibrium, albeit they acquire a privileged direction and are thus more ordered out of equilibrium. This happens because of the time asymmetric selection of initial conditions under nonequilibrium conditions, resulting into an invariant probability distribution which breaks the time reversal symmetry by favoring some trajectories with respect to their time reversal images. The temporal ordering is possible at the expense of the increase of the phase-space disorder and is thus compatible with Boltzmann's interpretation of the second law.

The time asymmetry of temporal disorder has been observed for driven Brownian motion in the aforementioned experiments [11,12]. Figure 5c depicts the forward and reversed randomnesses versus the rescaled resolution $\delta = \varepsilon/\sqrt{1-\exp(-2\tau/\tau_{\mathrm{R}})}$ where $\tau_{\mathrm{R}} \simeq 3$ ms is the relaxation time of the Brownian particle in the laser trap. First of all, we observe that these quantities increase as the resolution goes down to the scale of nanometers, reached thanks to the interferometric techniques [11,12]. This means that the stochastic process of Brownian motion generates more and more temporal disorder as the process is observed on smaller and smaller scales ε. For small values of the spatial resolution ε, we find that

$$h(\varepsilon,\tau) = \frac{1}{\tau}\ln\sqrt{\frac{\pi \mathrm{e}\mathcal{D}\tau_{\mathrm{R}}}{2\varepsilon^2}\left(1-\mathrm{e}^{-2\tau/\tau_{\mathrm{R}}}\right)} + O(\varepsilon^2) \tag{21}$$

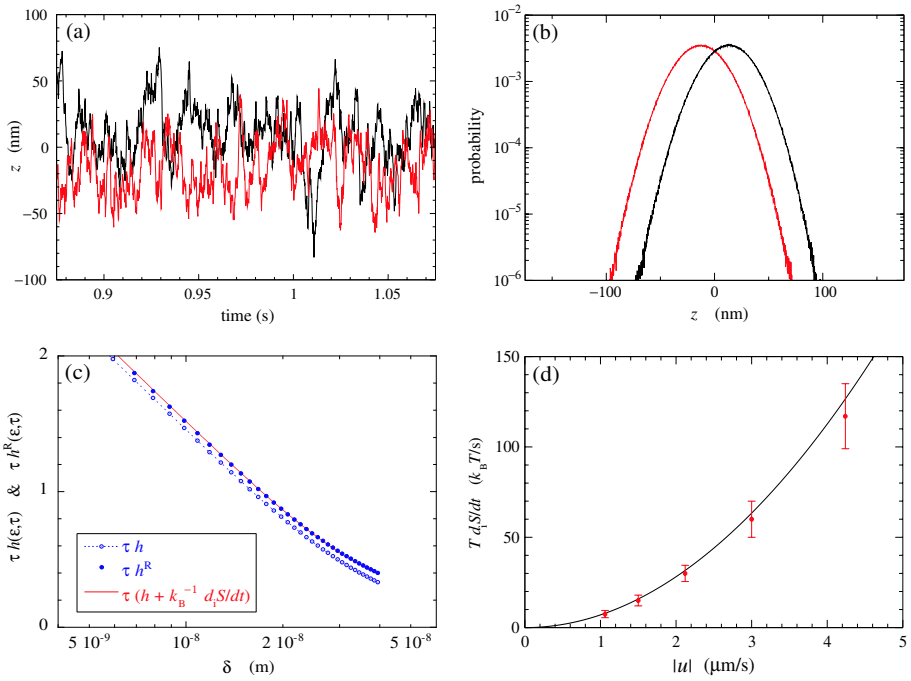

Fig. 5. (a) The time series of a typical path z_t of a trapped Brownian particle in a fluid moving at the speed u for the forward process (upper curve) and $-u$ for the reversed process (lower curve) with $u = 4.24 \times 10^{-6}$ m/s. The temperature is $T = 298$ K and the sampling frequency $f = 8192$ Hz. (b) Gaussian probability distributions of the forward and backward experiments. The mean value is located at $\pm u\tau_{\rm R} = \pm 12.9$ nm. (c) The rescaled forward and reversed randomnesses $\tau h(\varepsilon, \tau)$ and $\tau h^{\rm R}(\varepsilon, \tau)$ for $\tau = 4/f$ versus $\delta = \varepsilon/\sqrt{1 - \exp(-2\tau/\tau_{\rm R})}$. The solid line is the result expected from Eq. (20), showing the good agreement. (d) Thermodynamic entropy production of the Brownian particle versus the driving speed $|u|$. The solid line is the well-known rate of dissipation given by $d_{\rm i}S/dt = \alpha u^2/T$ where α is the viscous friction and T the temperature. The dots depict the difference $h^{\rm R} - h$ between the randomnesses. The formula (20) is thus verified up to experimental errors. The equilibrium state is at zero speed $u = 0$ where the entropy production vanishes. Adapted from Ref. [12].

where $\mathcal{D} = 1.4 \times 10^{-13}\,{\rm m}^2/{\rm s}$ is the diffusion coefficient of the Brownian particle [12]. The second important observation in Fig. 5c is that the reversed randomness $h^{\rm R}$ is larger than the forward randomness h by an amount equal to the thermodynamic entropy production in units of Boltzmann's constant. This is the manifestation of the time asymmetry of nonequilibrium fluctuations, which is here remarkably observed down to the nanoscale [12]. The difference between the reversed and forward randomnesses is quadratic in

the fluid speed u as expected from viscous dissipation (see Fig. 5d).

Similar results have been obtained for an RC electric circuit, showing the time asymmetry down to fluctuations of about a few thousands electronic charges [12]. The link between the formula (20) and the escape-rate theory has been discussed elsewhere [4]. The connection can also be established with nonequilibrium work relations [16,17].

5. The fluctuation theorem

Another newly discovered relationship is the fluctuation theorem which concerns the probability distribution of fluctuating quantities such as the currents crossing a nonequilibrium system, the corresponding dissipated heat, or the work performed on the system. Several versions of the fluctuation theorem have been derived for either dynamical systems or stochastic processes [18–23]. The fluctuation theorem is based on the microreversibility implying a symmetry relation between the probabilities of opposite fluctuations.

Recently, we have carried out a derivation of the fluctuation theorem for stochastic processes in the framework of the graph theory by Hill, Schnakenberg, and others [24–26]. This approach allows us to identify the thermodynamic forces – i.e., the De Donder affinities [27,28] – driving the system out of equilibrium [29–31]. In chemical kinetics, the affinities are given in terms of the free enthalpy changes of the reactions:

$$A_\gamma = \frac{\Delta G_\gamma}{k_\mathrm{B}T} = \frac{G_\gamma - G_{\gamma,\mathrm{eq}}}{k_\mathrm{B}T} \tag{22}$$

where T is the temperature [27,28]. In electric devices, the affinities are given by the difference of electronic chemical potentials between the electromotive sources of the circuit. If the affinities vanish, the system returns to equilibrium. Therefore, these affinities drive nonequilibrium currents, which take fluctuating instantaneous values $j_\gamma(t)$. The average of such a current over a finite time interval t is thus the random variable:

$$J_\gamma = \frac{1}{t}\int_0^t j_\gamma(t')\,dt' \tag{23}$$

In chemical reactions, these currents are the rates of the reactive events, i.e., the rates of the transformations of reactants into products. In chemomechanical systems such as the F_1-ATPase rotary molecular motor, a current may represent the number of revolutions per unit time while another is the rate of consumption or synthesis of ATP. Accordingly, the system may

sustain several currents $\mathbf{J} = (J_1, J_2, ..., J_\gamma, ..., J_c)$ driven by as many corresponding affinities $\mathbf{A} = (A_1, A_2, ..., A_\gamma, ..., A_c)$. For the molecular motor, these affinities are respectively the external torque acting on its shaft and the affinity of ATP hydrolysis (see below).

The fluctuation theorem for the currents asserts that the ratio of the probabilities of opposite fluctuations goes exponentially with the time interval and the magnitude of the affinities and fluctuations:

$$\frac{P(\mathbf{J})}{P(-\mathbf{J})} \simeq \exp\left(\mathbf{A} \cdot \mathbf{J}\, t\right) \qquad \text{for} \quad t \to \infty \tag{24}$$

The statistical average of the argument in the exponential is nothing else as the thermodynamic entropy production:

$$\frac{1}{k_{\rm B}} \frac{d_{\rm i} S}{dt} = \mathbf{A} \cdot \langle \mathbf{J} \rangle \geq 0 \tag{25}$$

The fluctuation theorem for the currents allow us to obtain the generalizations of Onsager's reciprocity relations to the nonlinear response coefficients [29,31].

If we introduce the decay rate of the probability as $P(\mathbf{J}) \sim \exp\left[-H(\mathbf{J})\, t\right]$, the fluctuation theorem can be expressed in the form:

$$\mathbf{A} \cdot \mathbf{J} = H(-\mathbf{J}) - H(\mathbf{J}) \tag{26}$$

which shows the similarity with the other new relationships that are the equations (13) and (20), as well as the escape-rate formulae [9,10]. If Eq. (26) is evaluated for the mean currents, the thermodynamic entropy production turns out to be given by $H(-\langle \mathbf{J} \rangle)$ since $H(\langle \mathbf{J} \rangle) = 0$. Comparing with Eq. (20), we infer that the reversed randomness is larger – and typically much larger – than the decay rate of the opposite current probability: $h^{\rm R}(\varepsilon, \tau) \geq H(-\langle \mathbf{J} \rangle)$. This shows that the probability distribution of the currents characterizes the system in a coarser way than the (ε, τ)-entropies per unit time, which can even probe the fluctuations down to the nanoscale [12]. In this sense, the fluctuation theorem is closer to the macroscale than the relationship (20) described in the previous section.

6. Molecular motors

The new advances reported in the previous sections apply to out-of-equilibrium nanosystems such as the molecular motors, characterizing the way they function in the presence of fluctuations. One of the best known molecular motors is the F_1-ATPase studied by Professor Kinosita and coworkers [32,33]. The F_1-ATPase protein complex is a barrel composed

of three large α- and β-subunits circularly arranged around a smaller γ-subunit playing the role of the shaft. The three β-subunits contain the reactive sites for the hydrolysis of ATP. A bead of 40 nm-diameter is attached to the shaft to observe its motion, which clearly shows that the rotation takes place in six substeps: ATP binding induces a rotation of about 90° followed by the release of ADP and P_i during a rotation of about 30° (see Fig. 6). Therefore, the hydrolysis of one ATP corresponds to a rotation by 120° and a revolution of 360° to three sequential ATP hydrolysis in the three β-subunits. There is thus a tight coupling between rotation and chemical reactions in this chemomechanical system.

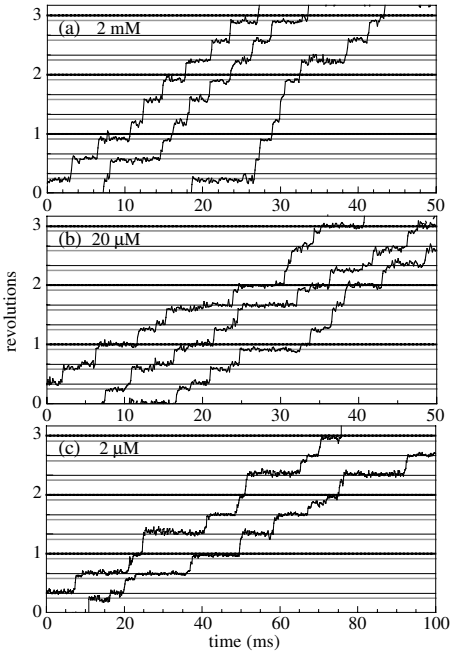

Fig. 6. Experimental data of R. Yasuda, H. Noji, M. Yoshida, K. Kinosita Jr., and H. Itoh [32] on the time courses of stepping rotation of the F_1 motor with a 40-nm bead attached to the rotating γ-subunit at: (a) [ATP] = 2 mM; (b) [ATP] = 20 μM; (c) [ATP] = 2 μM.

In the simplest approximation, the motor can be modeled as a stochastic process with six conformational states whether the sites of the three β-subunits are occupied or not [34]. The random transitions between these

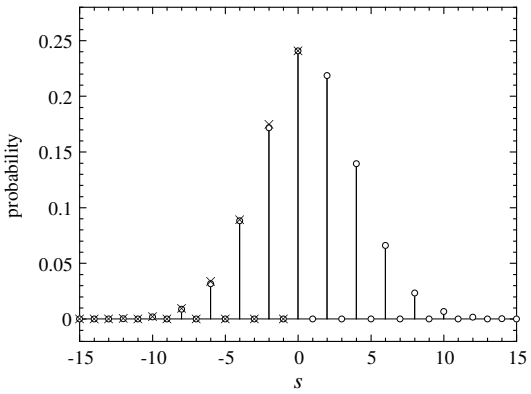

Fig. 7. Probability $P(s)$ (open circles) that the F_1 motor performs s substeps during the time interval $t = 10^4$ s compared with the prediction $P(-s)\exp(sA/6)$ (crosses) of the fluctuation theorem (29) for $[\mathrm{ATP}] = 6\ 10^{-8}$ M and $[\mathrm{ADP}][\mathrm{P_i}] = 10^{-2}\ \mathrm{M}^2$ corresponding to the affinity $A \simeq 0.6$ close to equilibrium [34].

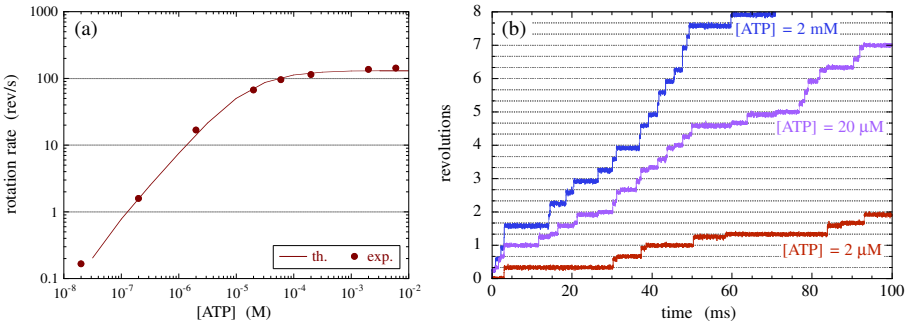

Fig. 8. (a) Rotation rate of the F_1 motor in revolutions per second versus the ATP concentration, under the experimental conditions $[\mathrm{ADP}][\mathrm{P_i}] = 0$, 23°C, and a bead of 40-nm diameter. The dots are the experimental data of Ref. [32] while the solid line is the result of the model of Ref. [35]. (b) Stochastic trajectories of the rotation of the F_1 motor simulated by the model of Ref. [35] under the same conditions as the experimental observations of Fig. 6.

states are due to the reactive events of the following chemical scheme:

$$\mathrm{ATP} + \mathrm{F_1}(\sigma) \rightleftharpoons \mathrm{F_1}(\sigma+1) \rightleftharpoons \mathrm{F_1}(\sigma+2) + \mathrm{ADP} + \mathrm{P_i} \quad (\sigma = 1, 3, 5) \quad (27)$$

with $\mathrm{F_1}(7) \equiv \mathrm{F_1}(1)$. The affinity driving the motor out of equilibrium is controlled by the concentrations of ATP and the products of hydrolysis

according to

$$A = -3\,\frac{\Delta G^0}{k_{\rm B}T} + 3\,\ln\frac{[{\rm ATP}]}{[{\rm ADP}][{\rm P_i}]} \tag{28}$$

in terms of the standard free enthalpy of hydrolysis $\Delta G^0 \simeq -50$ pN nm at pH 7 and 23°C [33]. The affinity vanishes at equilibrium where the concentrations reach their equilibrium ratio. Out of equilibrium, the affinity drives the rotation of the motor. The chemical scheme (27) shows that the mean rotation rate has a Michaelis-Menten dependence on the ATP concentration. Accordingly, the F_1 motor typically functions in a highly nonlinear regime far from equilibrium [34].

Thanks to the fluctuation theorem (24), we can determine the probability of backward rotation as the motor is driven away from equilibrium. We find that [34]

$$\frac{P(s)}{P(-s)} \simeq \exp\left(\frac{sA}{6}\right) \tag{29}$$

for the probability $P(s)$ of a rotation by a signed number s of substeps over a time interval t. A full forward or backward revolution happens when $s = \pm 6$. This fluctuation theorem shows that the probability of backward rotation is reduced by the exponential factor $\exp(-sA/6)$ with respect to the probability of forward rotation. Figure 7 compares the forward and backward probabilities in a situation relatively close to chemical equilibrium, showing the agreement with the prediction of the fluctuation theorem. However, because of the large value of the standard free enthalpy of hydrolysis, the backward substeps rapidly become very rare as the motor is driven in the highly nonlinear regime with $40 < A < 60$ corresponding to the physiological conditions. This result shows that functioning away from equilibrium provides robustness to the biomolecular processes, allowing unidirectional motions to overwhelm erratic motions. The basic mechanism is that the nonequilibrium constraints suppress the time-reversed paths responsible for the erratic motions leaving time asymmetric unidirectional motions, as explained in the previous sections.

The aforementioned model of the F_1 motor can be extended to include the continuous variation of the rotation angle, still keeping the six states of the chemical scheme (27) [35]. In this way, it is possible to reproduce not only the Michaelis-Menten dependence of the rotation rate on the ATP concentration, but also the substeps of the stochastic trajectories with great realism (see Fig. 8).

7. Conclusions and perspectives

Recent progress in nonequilibrium statistical mechanics has achieved the integration of thermodynamics with stochastic aspects in systems driven out of equilibrium. In this regard, the new results provide the basis for a nonequilibrium statistical thermodynamics of nanosystems bridging the gap between the emergent macroscopic phenomena and the molecular motions at the nanoscale. The integration of thermodynamic and stochastic aspects has been made possible thanks to the discovery of new relationships which all share the same mathematical scheme in which an irreversible thermodynamic property is given by the difference between two quantities characterizing the randomness of molecular motions. This scheme appears in the escape-rate formulae [9,10], Eqs. (13) and (20), as well as the form (26) of the fluctuation theorem. In this way, the thermodynamic entropy production can nowadays be understood as a time asymmetry in the temporal disorder of nonequilibrium fluctuations.

These relationships concern the unidirectional motions of nonequilibrium systems such as the driven Brownian motion and the F_1-ATPase molecular motor. Although their motions are erratic at equilibrium where opposite random steps have equal probabilities, they become unidirectional out of equilibrium by the time asymmetric suppression of backward steps, as explained thanks to the new relationships. These results open important perspectives in our understanding of biological phenomena on the basis of thermodynamics. Indeed, one of the main features of life is metabolism, which is the evidence of the many nonequilibrium processes taking place in cells. The recent results explain that this nonequilibrium regime is responsible for temporal ordering in the behavior of biosystems. In this way, modern statistical thermodynamics can give an answer to the question of the origins of order and information in biological systems.

Acknowledgments

This research is financially supported by the F.R.S.-FNRS Belgium and the "Communauté française de Belgique" (contract "Actions de Recherche Concertées" No. 04/09-312).

References

1. I. Prigogine, *Introduction to Thermodynamics of Irreversible Processes* (Wiley, New York, 1967).
2. P. Gaspard, *Chaos, Scattering and Statistical Mechanics* (Cambridge University Press, Cambridge UK, 1998).

3. P. Gaspard, *Physica A* **369**, 201 (2006).
4. P. Gaspard, *Adv. Chem. Phys.* **135**, 83 (2007).
5. P. Gaspard, *J. Stat. Phys.* **68**, 673 (1992).
6. S. Tasaki and P. Gaspard, *J. Stat. Phys.* **81**, 935 (1995).
7. S. Tasaki and P. Gaspard, *Bussei Kenkyu Cond. Matt.* **66**, 23 (1996).
8. P. Gaspard, I. Claus, T. Gilbert, and J. R. Dorfman, *Phys. Rev. Lett.* **86**, 1506 (2001).
9. P. Gaspard and G. Nicolis, *Phys. Rev. Lett.* **65**, 1693 (1990) .
10. J. R. Dorfman and P. Gaspard, *Phys. Rev. E* **51**, 28 (1995).
11. D. Andrieux, P. Gaspard, S. Ciliberto, N. Garnier, S. Joubaud, and A. Petrosyan, *Phys. Rev. Lett.* **98**, 150601 (2007).
12. D. Andrieux, P. Gaspard, S. Ciliberto, N. Garnier, S. Joubaud, and A. Petrosyan, *J. Stat. Mech.: Th. Exp.* P01002 (2008).
13. P. Gaspard and X.-J. Wang, *Phys. Rep.* **235**, 291 (1993).
14. P. Gaspard, *J. Stat. Phys.* **117**, 599 (2004); *Erratum* **126**, 1109 (2006).
15. P. Gaspard, *C. R. Physique* **8**, 598 (2007).
16. C. Jarzynski, *Phys. Rev. E* **73**, 046105 (2006).
17. R. Kawai, J. M. R. Parrondo, and C. Van den Broeck, *Phys. Rev. Lett.* **98**, 080602 (2007).
18. D. J. Evans, E. G. D. Cohen, and G. P. Morriss, *Phys. Rev. Lett.* **71**, 2401 (1993).
19. G. Gallavotti and E. G. D. Cohen, *Phys. Rev. Lett.* **74**, 2694 (1995).
20. J. Kurchan, *J. Phys. A: Math. Gen.* **31**, 3719 (1998).
21. J. L. Lebowitz and H. Spohn, *J. Stat. Phys.* **95**, 333 (1999).
22. C. Maes, *J. Stat. Phys.* **95**, 367 (1999).
23. G. E. Crooks, *Phys. Rev. E* **60**, 2721 (1999).
24. T. L. Hill, *Free Energy Transduction and Biochemical Cycle Kinetics* (Dover, New York, 2005).
25. J. Schnakenberg, *Rev. Mod. Phys.* **48**, 571 (1976).
26. D.-Q. Jiang, M. Qian, and M.-P. Qian, *Mathematical Theory of Nonequilibrium Steady States* (Springer, Berlin, 2004).
27. T. De Donder and P. Van Rysselberghe, *Affinity* (Stanford University Press, Menlo Park CA, 1936).
28. G. Nicolis and I. Prigogine, *Self-Organization in Nonequilibrium Systems* (Wiley, New York, 1977).
29. D. Andrieux and P. Gaspard, *J. Chem. Phys.* **121**, 6167 (2004); *Erratum* **125**, 219902 (2006).
30. D. Andrieux and P. Gaspard, *J. Stat. Phys.* **127**, 107 (2007).
31. D. Andrieux and P. Gaspard, *J. Stat. Mech.: Th. Exp.* P02006 (2007).
32. R. Yasuda, H. Noji, M. Yoshida, K. Kinosita Jr., and H. Itoh, *Nature* **410**, 898 (2001).
33. K. Kinosita Jr., K. Adachi, and H. Itoh, *Annu. Rev. Biophys. Biomol. Struct.* **33**, 245 (2004).
34. D. Andrieux and P. Gaspard, *Phys. Rev. E* **74**, 011906 (2006).
35. P. Gaspard and E. Gerritsma, *J. Theor. Biol.* **247**, 672 (2007).